NASA Technical Memorandum 83473

Relation of Cyclic Loading Pattern to Microstructural Fracture in Creep Fatigue

S. S. Manson
Case Western Reserve University
Cleveland, Ohio

and

G. R. Halford and R. E. Oldrieve
Lewis Research Center
Cleveland, Ohio

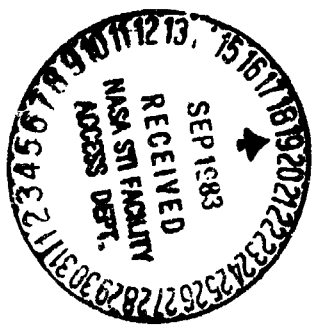

Prepared for the
Fatigue 84 (The Second International Conference on
Fatigue and Fatigue Thresholds)
Birmingham, England, Septemoer 3-7, 1984

NASA

RELATION OF CYCLIC LOADING PATTERN TO MICROSTRUCTURAL FRACTURE IN CREEP FATIGUE

S. S. Manson
Case Western Reserve University
Cleveland, Ohio 44106

and

G. R. Halford and R. E. Oldrieve
National Aeronautics and Space Administration
Lewis Research Center
Cleveland, Ohio 44135

SUMMARY

Creep-fatigue-environment interaction is discussed using the Strainrange Partitioning framework as a basis. The four generic SRP strainrange types are studied with a view of revealing differences in micromechanisms of deformation and fatigue degradation. Each combines in a different manner the degradation associated with slip-plane sliding, grain-boundary sliding, migration, cavitation, void development and environmental interaction; hence the approach is useful in delineating the relative importance of these mechanisms in the different loadings. Micromechanistic results are shown for a number of materials, including 316 SS, wrought heat resistant alloys, several nickel-base superalloys, and a tantalum-base alloy, T-111. Although there is a commonality of basic behavior, the differences are useful in delineating several important principles of interpretation. Some quantitative results are presented for 316 SS, involving crack initiation and early crack growth, as well as the interaction of low-cycle fatigue with high-cycle fatigue.

INTRODUCTION

It has long been recognized that metal fatigue, even at room temperature, is a very complex process. Yet, simple relationships have been developed to enable technologists to treat many engineering problems with relative ease and a high degree of accuracy (ref. 1). The main reason for the accomplishment of good engineering approaches is that, after a long history of controversy regarding the nature of the fatigue mechanism and its controlling variables (ref. 2), there has emerged the understanding that mechanistically, metal fatigue is primarily the result of plastic deformation associated with slip-plane sliding (refs. 3 and 4). Thus the important parameter is the amount of reversed plastic flow developed. While numerous other variables can also affect the ultimate response (ref. 5) -- such as environment, metallurgical state and stability, strain rates, mean and maximum stress, etc. -- the most profitable approach has been found to treat these variables as secondary, and to apply suitable modifications to the analysis which is based on local stresses and plastic deformations (ref. 6). Even where some controversy still exists as to whether it is more fruitful to lump the period during which an engineering-size crack (ref. 6) is generated, or whether to track by the laws of fracture mechanics the growth of the crack from a microstructural dimension to the final fracture of an engineering component (ref. 7), the focus is still

mainly on the generation and growth of a single dominant crack, and the variables controlling this event are mainly stresses and plastic strains.

With the introduction in the last two decades of technological applications involving loadings and loading reversals on metals at high temperatures, new ambiguities have again developed as to which variables are dominant, which are secondary in causing fatigue damage, and which, indeed, are the important and secondary micromechanisms associated with such damage. At high temperatures environmental interaction can become more pronounced both because of oxide penetration and associated metallurgical interaction, and because of coatings that can form microstructural instabilities associated with prolonged temperature exposure. Even without environmental interaction such instabilities can produce beneficial or detrimental effects. New modes of deformation in addition to slip-plane sliding can occur at high temperature, and the nature of the strain developed may depend on the imposed strain rate and what has transpired on the previous half cycle of loading. Because of alternative deformation mechanisms, new micromechanisms of fracture can develop -- common among them grain boundary cracking. Rheological response associated with high temperature can introduce mean and maximum stresses not normally encountered at room temperature, and such stresses may have significant effect on fatigue life. It becomes important to know which are controlling and which are secondary. The question also again arises as to whether it is appropriate to treat damage as the growth of a dominant crack from its microstructural size to the point of failure through a single set of crack growth laws, or whether a special treatment is required for the gestation period during which the dominant crack is generated. The mechanism of such crack formation may differ sufficiently from the mechanism of its growth to preclude treatment by a single law.

The state of technological development to treat high temperature fatigue reflects great uncertainty as to appropriate basic framework for analysis. There are at present a large number of competing methods, each featuring a different primary mechanism, with provisions for secondary effects. One method features environment and mean stress (ref. 5), others mean and maximum stress (ref. 8), crack growth and its interaction with grain boundary cavitation (ref. 9), the algebraic addition of individual damages due to creep rupture and fatigue (ref. 10), and the interaction of slip plane and grain boundary sliding (ref. 11). It is clear, therefore, that if valid design procedures are to evolve they must be based an improved understanding of what really does happen mechanistically during high temperature fatigue. Which framework among those outlined, if any, is more likely to be successful as a unified design method because it places the variables in the proper perspective and proportion. Or, is it possible that several frameworks are needed because various materials perceive the parameters differently?

In this paper we pursue in some detail a number of micromechanistic observations we have made using as our reference frame, the Strainrange Partitioning (SRP) concept. This method gives primary consideration to the interaction of grain boundary and slip-plane sliding. Our quantitative studies are only in their initial stages, and further measurements are in progress. However, we shall present in this report sufficient experimental information to be useful in explaining the relative importance of some of the micromechanisms of interest, and how some anomalous results that have been obtained in the past can be explained on the basis of the micromechanisms

observed. Although the main focus of the discussion will be on austenitic 316 SS, wrought heat resistant alloys, nickel-base superalloys and a tantalum-base alloy, T-111, will also be used to illustrate the concepts involved.

MICROMECHANISMS ASSOCIATED WITH THE STRAINRANGE PARTITIONING (SRP) FRAMEWORK

Although the SRP framework for technological analysis does not require the designation of any particular micromechanisms of damage, its conception was based on certain perceived combinations of microstructural deformation. In principle, certain types of localized damage should be associated with each of the generic strain ranges utilized in the method. Hence, we consider here first the idealized damage types to be expected, and subsequently the possible effect of secondary variables on damage generation.

The SRP framework is based on the existence of a bimodal system of deformation involving both slip-plane (SP) sliding and grain-boundary (GB) sliding. Slip-plane sliding[1] constitutes the more common form of plastic deformation observed at all temperatures, while grain-boundary sliding[2] takes on importance in the creep range at temperatures above approximately half the absolute melting temperature of the alloy. Plasticity, therefore, is inelastic deformation that can occur without GB sliding, just as it occurs during the plastic flow of most metals at room temperature. Creep, on the other hand, is inelastic deformation that involves, but is not limited to, GB sliding. Grain-boundary sliding by itself would normally introduce internal discontinuties. While such discontinuities do in fact occur, as evidenced by triple point cracks, not all of the internal displacements are accomodated by cracking. The grains may also distort by SP sliding, thereby accomodating some of the GB sliding while maintinaing structural continuum. We will define as creep that strain which is introduced by the GB sliding, but which may also contain both induced slip-plane sliding as well as internal structural dicontinuities. Thus, although the actual contribution of GB sliding to the inelastic strain may be quite small, the induced damage may be substantial[3].

---

[1]In the discussion that follows plastic deformation will be represented as SP sliding; it is understood that alternative mechanisms of room temperature deformation, such as twinning, can also be involved in such straining.

[2]Although for simplicity, we initially considered only sliding as the mechanism whereby GB participate in high temperature deformation, it is clear that there are ways other than sliding in which such participation can occur. One such way will be discussed later in this report. For brevity, however, we shall interpret the term GB sliding as a generic one which includes all mechanisms by which GBs contribute to inelastic strain.

[3]It can readily be shown that all the rules used in SRP analysis, for example the Interaction Damage Rule (ref. 12), are equally valid even when what is regarded as a creep strain is not pure GB sliding, but has associated with it any amount of plasticity, so long as the two remain in fixed proportion for all creep conditions.

Given, therefore, that there are two basic modes of deformation -- SP sliding which does not involve GB sliding, and GB sliding which is accompanied by enough SP sliding to maintain metal continuity (and a number of induced discontinuities) -- the SRP framework attempts to distinguish in nature of damage among the four permutations of deformation of closed hysteresis loops in which tensile strain is balanced by compressive strain: PP in which plastic flow in tension is balanced by plastic flow in compression, CC in which creep in tension is balanced by compressive creep, CP in which creep in tension is balanced by compressive plasticity, and PC in which tensile plasticity is balanced by compression creep. It can be seen that because of the differences in the nature of strain reversal, the possibility is considered that the damage mechanisms are generic, since they are strain combinations uniquely identified by the test cycles in which the damage is introduced. Thus the basis of the SRP method is to require a series of tests to be conducted in which the four unique combinations of creep and plasticity are interacted by associating them with the tensile and compressive halves of the cycle. While the method does not stipulate the precise loading to be used to accomplish such interaction, the implication is that the tests can be conducted to impose a major component of the desired type of strain in tension and compression. Furthermore, any cycle, for example, a diverse set of tests involving stress-hold, strain-hold, and temperature and strain variations which are either in-phase or out-of-phase with each other can be partitioned into its component strainranges for the purpose of predicting the cycle lifetime. A suitable interaction damage rule is postulated (ref. 12) to interpret the results when mixed strains are involved.

The SRP method requires only that a set of life relations be constructed for each of the generic types of strainranges. These life relations are then used in technological applications to calculate cyclic life for any selected loading pattern.

While the method recognizes that the differences in micromechanistic deformation and fracture are the reasons for singling out the generic strains as the units of interest in the creep-fatigue processes, it does not rely on a quantitative analysis, or even description, of these micromechanisms. However, in order to improve the usefulness of the method, and to point to future extensions, it is very useful to study some of these mechanisms in detail. In figures 1 to 4 we show these mechanisms schematically; in a later section we shall illustrate them for a variety of actual materials.

CP Loading

Figure 1 shows in exaggerated detail what happens in the vicinity of the surface of a specimen subjected to one CP loading cycle. As shown by the hysteresis loop the tensile load is applied for a time period required to produce a desired amount of creep. During this period the deformation is assumed to occur primarily by GB sliding (accompanied by SP sliding to maintain metal continuity). Voids may also develop by triple point wedge cracking, by grain particle fragmentation due to shearing, and as a result of the hydrostatic tensile stress component on boundaries normal to the applied stress. During the compression portion of the hysteresis loop the loading is imposed at a low temperature or is imposed rapidly with no time allowed for thermally activated GB sliding. Thus only SP sliding is added during the compression period. As

seen in the sketch of figure 1, such sliding near a previously displaced GB can result in an effective notch at the surface. The next application of the same hysteresis loop will produce a repetitive ratcheting, with increased GB sliding (together with required SP sliding) during the tensile half of the loop and increased SP sliding during compression. Of considerable importance when creep occurs is the activity that can take place in the GB which contributes to the inelastic strain. In our observations of a variety of materials these activities are of several types: (1) GB migration wherein the boundaries displace and rotate, producing more regularly arrayed networks of boundaries which become aligned for easier slip (for example with the 45° maximum shear stress direction), (2) GB cavitation resulting from the absorption of dislocations piled up against them, (3) GB cavitation resulting from dragging or fracturing of any GB particles, (4) GB cavitation due to the tensile stresses normal to the GB which enhance diffusion of vacancies to the boundary where they can agglomerate into voids and cracks, and (5) with sufficient GB sliding, high strain concentrations can develop wedge shaped cracks at triple points where the heterogeneity of strain distribution is maximized from grain to grain. On the basis of these phenomena it is expected that idealized CP straining will display the following characteristics:

(1) Notching at surface grain boundaries.

(2) Evidence of GB sliding and other GB activity such as migration, cavitation, etc.

(3) Triple point wedge cracking.

(4) Evidence of SP sliding due both to the plasticity during compression, as well as the reversed continuity-induced plasticity.

(5) Intercrystalline fracture, which can be common when cavitation predominates in the grain boundaries. Although not discussed above, it is recognized that oxidation can induce intercrystalline fracture by attacking surface connected grain boundaries. However, intercrystalline fracture is not a requirement of the SRP framework. Some materials fracture transgranularly even under long-time CP testing in air at high temperature, as will be discussed for the H-13 alloy.

PC Loading

In PC loading the compression is accomplished by the creep mechanism whereas the tension is by plasticity. The hysteresis loop and mechanistic features of PC deformation are seen in figure 2. In some respects the mechanisms involved are similar to CP loading. Grain boundary particles may crack and shear voids may form. Also, GB migration may occur to a limited degree, as can cavitation due to collections of piled-up dislocations. However, fewer voids are expected to grow, over a given time, strain range, and number of cycles, compared to CP straining because of the healing of cavities under compressive normal stress. Thus, while intercrystalline fracture is not precluded (and can in fact, occur, as will be illustrated) the tendency for such fracture is lower than for CP straining.

When an oxidizing environment is available, the PC type of loading can suffer more drastically than other types of loadings. The relatively long

time that the surface is subjected to compression permits formation of an oxide layer that is in equilibrium with the substrate. This oxide is then quickly cracked as the material is subjected to rapidly applied tensile strain during cooling. The dynamics of oxide penetration are complex, but as we shall later illustrate, the combination of long compression time and short tensile time produces serious environmental degradations due to oxide cracks that can then penetrate into the metal. On the basis of figure 2 and the discussion provided above, we can expect to see for PC loading:

(1) Notching at surface grain boundaries.

(2) Surface ledges or tongues due to sliding off along grain boundaries.

(3) Possible GB migration, sliding, and cavitation due to absorptions of piled-up dislocations (but less than in CP loading).

(4) Some triple point wedge cracking, but not as much as in CP loading.

(5) Evidence of monotonic tensile SP sliding, as well as reversed SP plasticity.

(6) A fracture path that is usually associated with the monotonic tensile plasticity combined with the induced reversed plasticity. Thus the fracture surface may look like that of an ordinary PP test, and may show striations developed as the crack grows under with the reversed plasticity.

(7) Under special conditions (as will be illustrated) intercrystalline cracking may occur, resulting from GB cavitation that forms from piled-up dislocations.

(8) Massive surface cracking (as will be illustrated) when tested in an oxidizing environment, starting in the surface oxide and penetrating the substrate metal.

(9) Some evidence of the presence of tensile mean stress. (As seen in hysteresis loop fig. 2 a higher stress is necessary to produce in a short time the tensile strain developed in a longer time during compression; thus the mean stress of the loop is tensile.) When the inelastic strain is small, comparable to the elastic strain, as in high cycle fatigue loading, the effect may be significant. One effect of such mean stresses could be to produce higher striation spacing (faster crack growth) during the crack growth period. For large inelastic strain the effect of mean stress is expected to be small (ref. 13).

PP Loading

Reversed plasticity loading, as illustrated in figure 3, shows a hysteresis loop similar to conventional fatigue at room temperature. The mechanism can be expected to be similar to that of room temperature fatigue. Cracking is due predominantly to slip-plane sliding which agglomerates imperfections into narrow slip bands. Although such sliding occurs within the slip planes of numerous interior grains, the crack almost always starts at the surface where the initiation is aided by surface irregularities, environmental enhancement, and the absence of the cohesive forces of atomic layers of metal

exterior to the surface. Cracks in the surface and near-surface grains usually start in the slip planes (Stage I (3)), and propagate normal to the applied stress (ref. Stage II (3)). Striations mark the cycle-by-cycle crack advance in low cycle fatigue.

While cracks do not commonly initiate in interior grains, the growth of the dominant crack is accelerated by the deterioration that has occurred by slip-plane weakening. On this basis we would expect to see, in PP loading, (1) little or no evidence of GB activity; (2) few, if any, triple-point cracks; and (3) cracking that starts at the surface and proceeds into the volume, with characteristics very similar to room-temperature fatigue: persistent slip bands, striations, etc.

CC Loading

The hysteresis loop and the mechanistic processes involved are shown in figure 4. When both tensile and compressive loadings are imposed for sufficiently long periods to allow equal creep strains in both the forward and reverse direction, some of the favorably oriented grain boundaries will be subjected to reverse sliding. Grain boundary migration may occur, as well as cavitation due to absorption of piled-up dislocations, hydrostatic tensile stress induced voids, and shear voids formed by the dragging of GB particles or particle fracture by shear. Some of the cavities formed during tension tend to be healed during compression; however, the healing of imperfections of all types may not be complete, because of the localized fracturing that had occurred during the tensile loading. Thus the driving tendency is for GB cracking to occur. When an oxiding environment is present surface oxide cracking may develop, particulary in the grain boundaries. The degree of surface oxide cracking is not as severe as for PC since for CC loading the oxide grows under alternate periods of tension and compression, developing a dynamic state of equilibrium consistent with this loading pattern.

These factors considered, we can expect to see

(1) Surface notches at the grain boundaries, rumpling of the surface, and preferential oxidation at these regions of discontinuity.

(2) Evidence of GB sliding, including triple point cracking. Within the interior volume, limited cavitation may occur, but not as severe as for CP loading.

(3) Considerable grain boundary migration leading to an orthorhombic grain structure, with boundaries rotating toward the direction of maximum shear stress, migration is most pronounced for the CC type of straining.

(4) Evidence of PP straining resulting from induced plasticity during cycles when continuum conditions require the generation of crystallographic slip while grain boundaries are sliding.

(5) Regions that show intercrystalline cracking, and other regions that show slip plane cracking, or regions that show a combination of both mechanisms.

THE SRP LIFE RELATIONS AND THEIR MICROMECHANISTIC SIGNIFICANCE

Over the more than a decade since SRP was first proposed (ref. 11), the life relationships for a number of materials have been studied by many investigators. Figure 5 shows a summary of the results for some of these materials. The figure shows results for only those materials which are useful herein in illustrating fundamental behavior.

A general observation that can be made among all the materials is that the SRP life lines are of the Manson-Coffin type, being linear on a log-log plot of cyclic life versus inelastic strain. Thus the SRP framework is a general extension of the room temperature behavior of most materials. These life relations may be distinctly different, or some may coincide. Consideration of their relative position, together with observations of associated deformation fracture models is of special value in interpreting micromechanisms of fracture and useful quantitative consideration.

Cases Demonstrating Environmental Degradation

Figure 5(a) shows a comparison of the SRP life relations at 1000° to 1400° F in air and in high vacuum for the iron-base alloy A-286. The life lines for the generic components are distinct and widely separated from each other, indicating that a bimodal deformation exists for this alloy. In vacuum the lives are about a factor of 10 higher than in air, suggesting the importance of oxidation both in initiating and propagating the fatal crack. It has long been demonstrated that even at room temperature, alloys susceptible to oxidation (e.g., aluminum) (ref. 14) are considerably degraded in fatigue life by air compared to vacuum. Figure 5(a) demonstrates that the degradation carries over to high temperature where oxidation is even more active, and in which the grain boundaries are even more likely to participate. We have discussed the reasons for such degradation (ref. 15) and have suggested how the short-time SRP life relations can be extrapolated to long-time through considering ductility measured in tensile and creep-rupture tests.

Cases in which the Life Relations are Distinctly Displaced

The A-286 results of figure 5(a) are typical of a number of materials in which there is a distinct displacement among the life relations. A reasonable interpretation of this result is that the hypothesized bimodal deformation behavior is actually present in such materials. Other materials we have studied that have such behavior are the tantalum base alloy T-111 of figure 5(b) and 316 SS of figure 5(c). We shall discuss 316 SS in detail later; the T-111 results are of special interest micromechanistically because they very clearly demonstrate the unique role of GB participation in vacuum creep-fatigue. These results were obtained by TRW, Inc. under NASA sponsorship during the early development of the SRP method. Since NASA had provided a facility to the TRW Corporation for testing high temperature fatigue in a space environment, it was logical to conduct the tests in the high vacuum chamber (10^{-8} torr) of this facility. Most of the results were reported in reference 16.

Isothermal testing of the T-111 consisted of low frequency (0.0065 Hz) continuous strain cycling that produced inelastic strains that were principally of the CC type. No PP-type tests were performed. Two types of thermal-mechanical tests were featured in these studies; both were performed at the cycling frequency of 0.0065 Hz used in the isothermal tests. In one, strain and temperature were cycled in phase -- that is, tensile strain was increased as temperature was increased, and compressive strain was applied when the temperature was decreased. Thus some of the applied tensile strain was absorbed as creep, while the compression strain was absorbed completely as plasticity since the temperature was too low to permit creep. The major strain, then, was of the CP type. In the other thermal-mechanical type of test the temperature and strain were varied out of phase, so that compressive strain was applied when the temperature was traversing the creep range; thus the strain induced was of the PC type.

Figure 6 shows the large amount of GB migration and cavitation for all the strain types involving creep. The wide appearing grain boundaries for CC strains indicate that these boundaries were moving during the cycling, as they attempted to align themselves in the direction of maximum shear stress (45° to axial stress direction, ref. 17). The path swept by the boundaries is delineated by cavities that are attributed to the absorption of piled-up dislocations at the grain boundaries associated with the SP sliding. Thus, figure 6 verifies the SRP concepts of how SP and GB sliding interact. Furthermore, the figure shows how GB gross cracking can occur under CP loading. Other CP tests of T-111, not shown, displayed triple point cracking, also a consequence of SRP considerations. Of major significance, however, is that the fracture surfaces of the PC and CC loadings were also intergranular, even though their lives were high relative to the CP loading at the same strainrange. Apparently the GB cavities eventually agglomerated and produced a continuous GB fracture network during the large number of cycles that could be tolerated by this alloy (see fig. 5(b)). Thus we observe that intercrystalline fracture can occur even in the absence of oxygen, and even under PC loading if conditions are propitious for allowing sufficient GB cavities to agglomerate and promote gross fracture. That a bimodal process of deformation is involved, described by the SRP framework, is evidenced by the distinctness of the SRP life lines.

Cases in which the Life Relations Coincide

A few materials have been observed in which grain boundary sliding is absent resulting in essentially no difference among the life relations. Such materials do not invalidate the SRP framework; on the contrary they supplement the method and extend the usefulness in revealing the micromechanisms of the creep-fatigue deterioration process. For these materials the SRP test results show that essentially only one mechanism of deformation is involved. While the framework is not really necessary to analyze creep fatigue, conducting the SRP generic tests is the very process for determining the basic fact that only one deformation mechanism prevails. The results for polycrystalline Mar-M 200 at 1700° F, figure 5(d), illustrate such a material. Every type of strain cycle produces the same lifetime. Micrographs of fractured samples are shown in figure 7. It is seen that fracture generally occurs along the dendrite boundaries. The grain boundaries of this material are so highly strengthened that no GB sliding occurs, and deformation takes place only within the grains. Apparently, the dendrite boundaries are embrittled by the SP sliding

(possibly the result of dislocation pile-ups) and fracture occurs along this weakest path. All fractures, regardless of strain type, are along the dendrite boundaries. Since only one deformation mode is operative, all four types of cycles produce the same life relation.

Cases in which only the PC Life Line is Low Relative to the Others

Of special interest are materials like the tool steel H-13 shown in figure 5(e). When tested in air at 1100° F, there is near-coincidence of the PP, CP, and CC lines; however the PC life line is considerably lower than the others. The implication is that there is really only one deformation mode, so that basically all the life relationships would coincide if it were not for the specially deleterious oxidation effect associated with the PC loading. As discussed earlier, the PC loading allows a heavy oxide buildup during the compressive creep, but this oxide is cracked during the rapid subsequent tensile plasticity. Conducting the SRP life tests is an effective way of learning that the deformation is monomodal, but that oxidation effects predominate under PC loading conditions. Figure 8 shows the micromechanisms of fracture of the H-13 under the four types of imposed strains. It is clear that only transcrystalline failure is involved, but that the resultant oxide layer for the PC loading is heavier than for the others. Cracks in the oxide serve as the nuclei for subsurface cracks in the metal (fig. 8(b)). Thus, although the bimodal aspects of the SRP framework are not required for the creep fatigue analysis, the SRP generic test types reveal the conditions under which special precaution is required to avoid oxidation degradation.

It is interesting that the PC line is lower than the others for this material, while for the Mar-M 200 material no such degradation of the PC behavior occurs, as discussed in the previous section. However, it should be noted that H-13 is an iron base alloy subject to considerable oxidation at 1100° F while Mar-M 200 is a highly alloyed nickel-base material, quite resistant to oxidation even at the 1700° F test temperature.

Cases in which Creep Deformation is Beneficial

An unusual case of material behavior is illustrated in figure 5(f) for IN-792. Here the CP and CC life relations lie above the PP and PC lines (ref. 18). Thus, for this material tensile creep is actually beneficial, contrary to our usual experience which reflects that tensile creep is the more damaging type of deformation. In order to understand this result calculations were made using ductility-normalized life relations. Such relations have been suggested in reference 13, and refined in reference 19. To estimate PP and PC life lines use is made of the true ductility in the conventional tensile test; for estimation of the CP and CC life lines use is made of the ductility as measured in a creep-rupture test at the same temperature and approximately the same duration as expected in the creep-fatigue test (the calculation requires some trial and error calculations to match the test times). It so happens that for IN-792 the creep rupture ductility used in the calculations was actually higher than the tensile-test ductilities. Calculated life relations shown in figure 9 are superimposed on the experimental lines. Indeed, the calculations agree with the observations, and suggest that CP and CC actually should yield higher lives than PP and PC. Thus the usefulness of the SRP

framework is verified by this application. It has not been possible to study the micromechanisms involved because no metallography was conducted for these limited tests. Such tests could prove very revealing. Again, the adverse performance of PC relative to the others is not pronounced for IN-792, probably because of its good oxidation resistance at the temperature of testing.

Relation Between Deformation Mode and Fracture Mode

The deformation mode governs to a considerable extent the type of fracture which results. However, other factors also contribute, so there is no pure one-to-one relationship between them. The governing fracture mode depends on at least three important factors, described in the following sections:

Aspects relating to type of straining. - Since the type of strainr·nge to which the material is subjected tends to govern the type of fracture that develops, the same material can fail in either a transcrystalline or an intercrystalline fashion depending on the nuances of loading. For AISI 316 SS in air, for example, PP loading induces transcrystalline failure, CP distinctly intercrystalline, CC a combination of transcrystalline and intercrystalline, and PC a transcrystalline failure initiating at oxidation cracks. The SRP framework thus provides a basis for expectation and for analysis of failure by post-mortem examination.

Aspects relating to basic microstructural characteristics. - While some materials, like 316 SS, respond readily in fracture characteristics according to loading, others are less responsive to fracture alternatives because of inherent microstructural features. The MAR-M 200 permits no GB deformation, and as seen in figure 5(d), the life relationships reflect the monomodal deformation mechanism. The resulting fracture mode is totally intercrystalline, however. Apparently the brittle nature of the grain boundaries induces the fracture along these boundaries rather than within the grains. The discontinuities of strain at these boundaries and intersecting slip planes produce sufficient stress concentration to initiate fracture because of the low fracture toughness of the boundaries.

In the case of IN792 + Hf, figure 5(f), the CP and CC life relations lie above the PP and PC; an unusual behavior that readily can be explained within the framework of SRP. Based upon the fractographic and transmission electron microscopy reported by Annis, et al. (ref. 12), it is evident that the PP deformation occurred by crystallographic slip within grains. However, only so much SP deformation can be accommodated at the intersections with the grain boundaries before the intense concentration of stress initiates brittle fracture within the boundaries. In this respect, the behavior is no different from MAR M-200 discussed above. On the other hand, CP straining permits an additional mechanism whereby within-grain deformation is assisted by the presence of stacking faults which disperse the imposed strain among a larger number of slip planes. The resulting ductility, therefore, is higher in a creep test than in a rapid tensile test. Consequently, in a CP type test, the strain is absorbed more within the grain, and hence those slip planes that do intersect the grain boundaries produce lower stress concentration, and in turn, fewer intergranular fractures. The resultant larger number of cycles of straining that are permitted, thereofre, eventually agglomerate a sufficient number of fractures within the slip planes to introduce some evidence of

transgranular cracking. Thus, the final failure mode for CP loading contains a mixture of transgranular and intergranular elements.

It is interesting, therefore, that for this alloy, the separation of the life relations reflects not a bimodal deformation behavior, but two levels of ductility within one mode of deformation, transgranular. The intergranular fracture is a reflection, not of deformation within the grain boundaries, but of the development of a number of localized strain concentrations at the intersection of slip planes and grain boundaries, resulting in sequential fractures at various points along the grains. The transgranular fractures in the slip planes for a test involving tensile creep are a reflection of the larger number of reversals permitted by the strain dispersal mechanism.

Another, very important aspect of fracture relates to the metallurgical instabilities that can develop at high temperature, particularly when reversed strain is present. In some materials phases may dissolve with the matrix if strain reduces their size sufficiently; in other materials phases may precipitate -- when these phases are hard and brittle the result can be brittle fracture. It is not uncommon, for example, for the fractures of long time creep rupture tests to display intercrystalline fracture. However, comparably long time fatigue tests have not been conducted as yet. It will be interesting to observe the metallography of such tests.

Aspects relating to environment. - Hostile environments can attack surfaces, producing geometrical surface discontinuities that are detrimental to fatigue. The resulting chemical compounds that form may also be weak, and induce fracture. Or the hostile element, such as oxygen, can penetrate the subsurface, attack the grain boundaries, or induce precipitation of metallurgical phases that alter the fatigue characteristics. Thus, as seen in figure 5(a), an air environment is very detrimental to fatigue in all the modes of deformation in A-286 in the creep range. Usually the effect is to embrittle the material in the grain boundaries, so it is more common to observe intercrystalline fracture in an air environment than in vacuum. However, a hostile environment is not necessary for intercrystalline failure to occur. The tantalum alloy, T-111, characterized in figure 5(b) for tests at 1150° C in a high vacuum, also showed intercrystalline failure in the PC mode of deformation. Grain boundary sliding and fracture was evident in the metallurgical studies.

Finally, it should be pointed out that environment can induce a mixed-mode of fracture when changing conditions develop as the fracture progresses. In PP loading of 316 SS in air at 1200° to 1300° F, we have observed, for example, that the initial fatigue sites are surface intersections of grain boundaries. Oxygen attacks these weak sites and develops pits that initiate the fatigue. However, as the crack grows below a depth of a grain or two, the stress concentration provides the driving force for further growth of the cracks in directions related to stresses rather than to the paths of grain boundaries. Thus the further growth of the crack is intercrystalline although its rate of growth may still be aided by formation and fracture of oxides at the tip of the cracks under the cyclic loading. We shall illustrate this behavior later in the report.

We conclude therefore, that environment can significantly affect both the formation and growth of cracks, usually contributing to intergranular fracture, but that intergranular fracture can also occur, at least in the CP mode

and PC mode (under certain conditions), even in the total absence of hostile environment. Furthermore, even if a hostile environment assists the formation of intergranular surface sites of attack, the further growth of the cracks may better reflect the fracture characteristic associated with the loading pattern than the initial types of fracture. Thus, PP loading, which is inherently transgranular in 316 SS, may show some intergranular surface fracture sites at initiation points, but the major growth of the crack is transgranular.

NEW STUDY DIRECTED AT QUANTITATIVE OBSERVATIONS AND MEASUREMENTS FOR 316 SS

In order to augment our understanding of the micromechanisms of creep fatigue we are currently engaged in an extensive test program in which these mechanisms are studied by various microscopic means. Quantitative measurements of crack generation and early growth are also made and compared with expectations based on several methods. These studies involve examination of surface at various points during the lives of specimens subjected to each of the generic SRP strainrange cycles, periodic interruption of such loadings to section the specimen in order to study progress of defects in the interior, and examination of the fracture surface and cross-sectioning after fracture to study interior defects. While the program is not yet complete it is appropriate to present here some preliminary results which have led to a better understanding of the micromechanisms of creep-fatigue degradations for 316 SS.

The life relations for an earlier heat of this alloy are shown in figure 5(c). That a bimodal type of deformation prevails is evident from the wide separation of the life lines. It was, in fact, the extensive study of this heat of 316 SS in our early studies that led to the adoption of the SRP concepts. Figure 10 shows, for example, the results of one of our first tests (ref. 11), in which approximately equal strainranges of PC and CP type were applied to specimens. The PC failure was transgranular and life was nearly 20 times longer than the CP specimen which displayed a totally intergranular fracture. The currently used heat of 316 SS differs slightly in composition, method of manufacture, and heat treatment compared to the original material. Preliminary tests suggest that creep fatigue is somewhat less damaging to this heat than the earlier one; however, complete characterization of the current material is still in progress. In the following discussion some of the available results will be presented.

Microscopy and Fractography

Figures 11 to 14 show the results of microscopy studies for each type of strainrange. Each figure contains four views. View A is a schematic diagram of the major features we observed from study of many optical and scanning electron micrographs. Other views show the surface or interior section at some point during the progress of the test. The fracture surface is shown for one test.

PP loading. - For austenitic stainless steels and other similar alloys which permit easy slip, the PP cycle introduces predominantly crystallographic slip deformation (ref. 20). Thus in figure 11(a), the schematic shows classical slip-banding and transgranular cracking of the PP cycle. The direct

association of slip banding and crack-progression striations is evident in figures 11(b) and 11(d) where the slip planes, particularly within the surface connected grains, are decorated by carbide precipitation and, possibly, oxidation (ref. 21).

An interesting observation of the specimen surface during high temperature, high frequency loading in air is the role of the environment in initiating intergranular cracking (fig. 11(b)). By interrupting the test at 20 percent of life, polishing to remove the thin oxide film (short time at temperature), and electropolishing and etching, we have been able to observe that the oxide at the surface grain boundaries serves as the primary site of the crack initiation. Slip bands revealed by etching also appear to be associated with initiation sites. However, as the cracks grow inward beyond one grain depth, they propagate in a transgranular manner with pronounced striations (fig. 11(d)). Thus, while intergranular cracking associated with environmental interaction is always the apparent cause of crack formation, such intergranular attack has little influence on the crack growth beyond a grain or two below the surface. The mechanism of growth, once the cracks have started at intergranular surface sites, is very similar to that at room temperature wherein intergranular cracking is rarely seen. Enhanced oxidation may of course contribute to faster crack growth, but not by favoring grain boundaries.

PC loading. - Figure 12 shows the results for PC loading. As seen in the schematic of figure 12(a), surface cracks start by continued penetration of oxide cracks, as discussed earlier. The interior shows, however, occasional GB cracks due to compressive GB sliding (ref. 22), and even a few triple point cracks (ref. 23). These features contribute to crack growth; however, it is the oxide-induced crack that appears to initiate the cyclic fracture process. Thus the PC life is lower than that for PP because of more severe oxide cracking and internal deterioration due to GB participation in the deformation process.

The severity of the oxide cracking is demonstrated in figure 12(b), which shows the surface at 40 percent of life for 1 percent inelastic strainrange. Extensive birchbark type cracking is seen, the general direction being perpendicular to the axis of tensile loading. After the surface oxide is removed by subsequent polishing (at 75 percent of life) the deepest subsurface cracks remain in the metal matrix (fig. 12(d)) and are filled with oxide. At this stage crack depths are, however, significantly less than half the surface crack length. Hence, the aspect ratio (depth:length) of these environmentally assisted PC type transgranular cracks is significantly different from the aspect ratio (approximately 0.5) for classical fatigue-initiated PP type cracks. At a relatively lower inelastic strainrange of only 0.4 percent (fig. 12(c)), the PC cracking is similar to that for PP cycling, except for some evidence of grain boundary and secondary slip band cracking. Surface cracks result in additional surface grain boundary deformation at a large inelastic strainrange of 4 percent as shown in figure 12(e). The bent slip lines probably result from the carbide precipitation decoration of linear slip bands which are later crossed by secondary slip on which precipitation has not occurred. Of special interest is the surface ledging, or tongue formation, seen in figure 12(f), which verifies the deformation hypothesis shown schematically in figure 2.

In summary, PC cracking for 316 SS is characterized by multiple oxide cracking initiated in the surface, striations characteristic of slip-plane sliding and possibly more rapid crack growth than for PP because of the contributions of interior GB deterioration.

CP loading. - The schematic diagram of figure 13(a) shows considerable intergranular cracking both on the surface and in the interior of the material. Severe cavitation and a large number of triple point cracks are evident throughout the volume. Surface oxidation occurs, particularly at grain boundaries, and surface cracking starts from these oxides, although the oxidation and oxide cracking is not as severe as in PC loading. Of special interest, however, is the evidence of considerable slip-plane sliding, partly due to the monotonic compressive plastic flow inherent in CP straining, and mostly due to reversed slip-plane sliding induced by continuum consideration during GB sliding.

Surface oxidation at grain boundaries is seen at multiple points in figure 13(b) even after only 10 percent of life. These cracks penetrate the interior and merge with independently formed GB cracks throughout the volume. The final fracture surface is totally intergranular as already shown in figure 10 for another heat of this material.

Evidence of slip-plane sliding is seen in figure 13(c) where these slip planes are decorated during etching. The figure also shows grain boundary cavitation, but no massive decohesion. Grain boundary fracture of properly oriented grains does occur, however, as seen in figure 13(d).

For austenitic stainless steels the CP loading is by far the most damaging. Displacement of the life relations relative to each other is clear evidence of the bimodal deformation possible in these materials, and the metallographic evidence of figure 13 clearly shows the role of grain boundary activity and its interaction with slip-plane sliding (ref. 24). These factors, together with oxidation, cause a life reduction of 25 relative to pure fatigue loading.

CC loading. - For reversed creep loading both intercrystalline and transcrystalline fracture are seen in the schematic diagram of figure 14(a). The intercrystalline fracture results from the reversed GB sliding, but the damage is not as severe as in CP loading because of the healing effect of reversed sliding. Reversed SP sliding is also present because of continuity-induced slip. Thus, cracking can be due to fracture in the grain boundaries, fracture in the slip planes, or a combination of the two. As seen in figure 14(a) an intercrystalline crack sometimes merges with a transcrystalline crack, extending the total crack length. It is not surprising, therefore, that sometimes intercrystalline cracking predominates, sometimes transcrystalline (ref. 25). Studies on 304 SS by Majumdar and Maiya (ref. 26) showed reversed creep to produce only transgranular failure. They therefore incorporated in their Damage Rate life prediction method the concept that reversed inelastic strain heals all grain-boundary cavitation, contrary to our observations of the presence of grain-boundary cracking. It is possible that subtle differences can exist between the stainless steel used in their studies and in ours, suggesting that the nature of the CC loading is very sensitive to these factors. Surface oxidation is an important contributor to crack initiation as seen in figure 14(b). Oxidation of both intergranular and transgranular fractures

also is present. That CC transgranular cracking is identified with SP sliding is seen in both figures 14(b) and 14(c). Also seen is evidence of intergranular CC crack initiation (fig. 12(b)) and triple point wedge cracking on the surface (fig. 14(d)).

Thus it can be concluded that for CC loading of a material which displays bimodal deformation, both transgranular and intergranular fracture mechanisms can occur. The GB mechanisms are not as severe as for CP loading, because of the tendency toward healing by the reverse GB slip. Generally the damaging effect of a CC strain is more severe than a PP strain of the same magnitude.

Quantitative Analysis of Crack Initiation and Growth

A major objective of the current investigation is to provide a micromechanistic background for use in quantitative anaysis. While the SRP method requires that a set of life relations be provided, and while these life relations are usually adequate for making a life analysis, certain questions can arise in which a micromechanistic understanding can be of great value. For example, if the same CP, PC, or CC strainrange is induced by a stress-hold test or by a strain-hold test, will the life be the same? Or, if the same strainrange is induced in a short time or in a long time, will the results be the same? Over the decade that we have been studing SRP we have been able to answer some of these questions. For several questions the answers are still in doubt. Thus, the spirit of our current program is to combine analytical techniques with micromechanistic observations in order to provide a baseline of experience for answering many current issues. Typical of this type of approach is that of Priest and Ellison (ref. 27), who have suggested modifications to SRP on the basis of micromechanistic evidence and have improved test predictability. Our program is just in its initial stage; however, some of the information obtained to date may be of interest.

Relation between initiation and fracture. - One of our first attempts to quantify our measurements has been to check the validity of a relation we have developed (ref. 28) for use in cumulative fatigue damage analysis.

$$a = a_0 + (0.18-a_0)\,(N_a/N_f)^{(2/3)(N_f)^{0.4}} \qquad (1)$$

The term a_0 refers to initial size of a defect in the microstructure, and can, for practical purposes, be taken as zero. Thus equation (1) provides the crack depth a in inches developed after N_a cycles of a loading for which the fracture life of a conventional fatigue specimen would be N_f. We have applied the equation in two ways.

In figure 15 is shown a nomogram based on equation (1). The straight line represents the failure line for any type of test. The curved line is the calculation from equation (1) based upon a crack depth of 0.005 inch. A few data points are shown which are actual measurements for the indicated SRP strainrange wherein crack type depth is 0.005 inch (ref. 25). While there is some scatter, it is seen that agreement between calculation and measurement is reasonable. The equation already takes into account the nucleation period, and deals essentially with the growth of a dominant crack after it has reached

some engineering size as established by the choice of a. Although the mechanisms for nucleation of the cracks are quite different for each of the strainrange types, the points fall reasonably on the same curve. Thus figure 15 suggests that equation (1) may be useful for high temperature creep-fatigue analysis, even though its original derivation related to materials tested in the subcreep range where only slip-plane plasticity was active in initiating and propagating the crack. The value of N_f, however, incorporates all the specialized micromechanisms pertinent to each type of strainrange and must be determined independently following the requirements of the SRP method.

A second use of equation (1) is shown in figure 16. Here the surface crack length for each type of strainrange is plotted against life fraction. This length is calculated from equation (1) using the known fatigue life for the particular strainrange. Since for this plot we are relating the crack length along the surface rather than its depth, an empirical conversion factor developed from other studies is incorporated, taking the crack length as about two times the depth. Experimental points as measured on the surfaces of the specimens tested are then plotted in figure 16. Because the data are quite limited, the results must be considered preliminary. However, it is interesting that agreement between the calculation and experiment begins to occur only after the crack has grown to some relatively large size. In the early growth the measured cracks are considerably longer than would be expected if based on equation (1). A possible reason for the discrepancy is that the early cracks are usually the result of oxidized grain boundaries. Thus the crack length becomes the whole length of the contiguous boundary that can easily be attacked, and is unrelated to the number of applied cycles. The severity of the degradation due to these cracks is not as great, however, as it would be if they were induced by the normal fatigue mechanisms. Thus the cracks grow in depth slowly at first, and only later do they catch up with the requirements of equation (1). This question requires further study, particularly for the PC type of strainrange which, as already discussed, suffers more from oxidation cracks than do the other strainrange types.

Cumulative fatigue damage. - Equation (1) was originally developed (ref. 28) for special use in cumulative fatigue damage analysis, providing a basis for each of two methods -- the Damage Curve Approach (DCA) and the Double Linear Damage Rule (DLDR). The basis of the DCA is shown in figure 17, and has been classically applied for many years in cumulative fatigue analysis. The curves represent damage accumulation as a fraction of cycle ratio for two levels of loading. If a cycle ratio (n_1/N_1) is applied at the first level, and then loading is shifted to the second level, the progression is made by moving from point A on the N_1 curve to point B and the N_2 curve at constant damage. What is left to be used at the N_2 level, then, is the cycle ratio from B to 1.0. The merit of equation (1) in implementing the DCA is that it provides a simple analytical expression for constructing the curves OAF and OBF. The DLDR is a variation of the DCA and has the merit of simplifying the analysis for multiple loading levels, while yielding approximately the same results.

A recent application of the concept has been made on 316 SS using two sequential loadings in order to simulate an important current technological application. The problem is illustrated in the insert in figure 16. A number of out-of-phase strain/temperature hysteresis loops, simulating thermomechanical loading and developing primarily PC strain is imposed in the material

(life to failure at this loading is about 600 cycles). Subsequently the material is subjected to a large number of low-amplitude, high-frequency cycles (of strain amplitude such that life would be approximately 400 000 cycles). The problem is the determination of the interaction of LCF and HCF applied in sequence at high temperature. While we have applied the DCA and DLDR to many problems of this type, all prior applications involved mechanical loadings at lower temperatures for both loadings. The question here was whether a thermomechanical PC loading could be treated in the same way as a mechanical loading of the same lifetime, and whether temperature and temperature variation effects were important.

Figure 18 shows the results of several tests conducted to date. A plot is made of the remaining HCF cycle ratio against the imposed LCF cycle ratio. The curved line represents the predictions based on equation (1). The DLDR prediction is numerically similar, but the curve is replaced by two straight line segments (not shown). The data points are experimental values of the combinations of LCF and HCF cycle ratios responsible for failure. It is seen that good agreement develops between calculations and experimental results. Of great interest is how damaging a few LCF cycles can be in reducing the available HCF lifetimes. This subject requires further study, particularly of the micromechanisms involved, and is being pursued in our laboratories.

DISCUSSION

In this report we have examined a number of micromechanisms of fatigue in the creep range for several alloy systems including austenitic stainless steels, wrought heat resistant alloys, nickel-base superalloys, and a refractory tantalum-base alloy. Many complex mechanisms contribute to metal degradation including slip-plane sliding, grain-boundary sliding and migration, cavitation, surface notching, and environmental attack. These mechanisms can interact, producing a variety of resulting effects that govern cyclic lifetime in a complex manner.

We have proposed idealized cyclic deformation and cracking models for creep-fatigue-oxidation interactions that feature the micromechanisms associated with the alloy systems studied. These models are compatible with, and in some cases even derived from, the Strainrange Partitioning framework that has been found particularly useful in the formulation of the types of experiments that can most readily reveal the fundamental nature of material cyclic deformation response and the cataloging of the significant damage mechanisms. It is found, for example, that when the life relations for the generic SRP components all coincide, the implication is that a monomodal deformation mechanism predominates, but when these relations differ appreciably a multimodal (ideally bimodal) deformation system is likely operative. If three of the four life relations coincide, but one (PC) is appreciably lower than the others, an important oxidation deterioration mechanism or tensile mean stress governs in the maverick strainrange.

The SRP framework has been quite helpful in the interpretation of situations for which the introduction of creep actually prolongs cyclic life. The beneficial effect on life of the addition of tensile creep strain in the alloy IN 792 was caused by a dispersal of the imposed deformation and thus a reduction of the highly localized strains that are associated with crack initiation. Other notable life prediction methods such as the Time- and Cycle-Fraction

Rule, Damage Rate Approach, Continuous Damage, and Frequency Separation are at odds with the behavior observed for such an alloy.

The SRP framework has also contributed to the better understanding of environmental effects and their interaction with cyclic deformation modes. While the fine details of the interactions are extremely complex, we have been able to identify some important trends which would have been obscured had not the SRP methodology been applied. As a specific example, the poor resistance to PC cycling, when PC is the only deviant of the four SRP life relations, may be due in part to mean tensile stress effects for very small hysteresis loops, but for larger loops is clearly associated with the formation of surface oxides during the compressive creeping times that crack in a brittle manner during the rapid excursion into tension. These oxide cracks penetrate into the substrate and result in early crack initiation. The reverse condition of a CP cycle does not result in the brittle cracking phenomena since the oxide grows during the tensile portion of the cycle and undergoes rapid excursions into compression. The brittle surface layer is naturally more tolerant of compression than tension. In a CC cycle, the oxide layer forms alternately in tension and compression in such a manner that an equilibrium state of stress and strain is achieved within the oxide that is much more resistant to brittle cracking by the alternate excursions into tension and compression.

Another aspect of environmental and deformation related effects that has been made clearer by adopting the SRP approach is the role of vacuum. Not only does the vacuum environment promote increases in cyclic life for each of the four SRP cycles, it also permits, as a result of the greater number of accumulated cycles, additional mechanisms of cracking. As a specific example, for the ductile tantalum alloy T-111, the PC cycle in vacuum resulted in an intergranular cracking mode that was not associated with an appreciably foreshortened life. This resulted because intergranular cracking was promoted, not by the more classical manner of void growth in the grain boundaries caused by sliding or hydrostatic tension, but likely by a dislocation pile-up and collapse mechanism. The pile-up at grain boundaries would occur during tensile plastic straining and the collapse would take place during the compressive hold ng periods.

In addition, it has been demonstrated that a crack growth law that had been derived on the basis of room temperature behavior and was the basis for the DLDR is also applicable, at least partially, at elevated temperatures. Results presented for 316 stainless steel at 1300° F show that the PP, PC, and CC SRP cycles can be described by the cracking law which relies on the cyclic advance of a single dominant crack. Since cyclic crack advance during CP loading could not be measured (likely because of the linking up of numerous tiny intergranular crack sites distributed throughout the susceptible volume), it was not possible to compare predicted and observed cracking for this mode of cyclic loading. Because of the applicability of the crack growth law to PC and PP loading, it was possible to successfully apply the DLDR to two-step loadings involving out-of-phase thermal-mechanical strain cycling (PC + PP) followed by rapid cycling (PP) to failure. Whether the DLDR would apply to an in-phase thermal-mechanical strain cycling (CP + PP) condition remains to be seen.

The goal of this study has been to provide a baseline of information that can be useful in applying creep-fatigue technology to practical problems encountered in service. Of special importance is the question of how to use

information from one kind of test to predict behavior in another, especially where extrapolation in time is required. For this purpose it is desirable to combine micromechanistic information with engineering methodology in order to maximize the probability of successful prediction. While our program is just in its initial phase, it appears that the approach can contribute to our goals.

CONCLUSIONS

The following conclusions can be drawn from our study of the cyclic deformation and cracking mechanisms observed in a variety of alloys subjected to high-temperature, creep-fatigue-oxidation environments. Among the alloys studied in the program were types 304 and 316 Stainless Steel, A-286, H-13 Tool Steel, IN-792 + Hf, MAR M-200, and the Tantalum Alloy T-111. Air and vacuum environments were involved, and each alloy was tested at elevated temperatures high enough to promote thermally activated creep mechanisms.

(1) The Strainrange Partitioning (SRP) framework is compatible with the numerous cyclic deformation and cracking mechanisms that are present during creep-fatigue-oxidation exposure of high-temperature alloys.

(2) Idealized cyclic deformation and cracking models have been proposed that represent the observed micromechanisms.

(3) A crack growth law, originally derived from room temperature fatigue behavior, has been shown to be applicable quantitatively to high-temperature, creep-fatigue loadings involving PP, PC, and CC type SRP cycles. Applicability to CP type cycles could not be determined since these cycles did not yield information suitable for crack growth measurement.

(4) The double linear damage rule for cumulative fatigue damage analysis, which has its basis in the room temperature crack growth law, was demonstrated to be applicable quantitatively to creep-fatigue loading conditions involving PC and PP type loading cycles.

REFERENCES

1. Manson, S. S.: Fatigue: A Complex Subject - Some Simple Approximations. Exp. Mech., vol. 5, no. 7, 1965, pp. 193-226.

2. Gohn, G. R.: Mechanism of Fatigue. Mater. Res. Stand, vol. 3, no. 2, Feb. 1963, pp. 106-115.

3. Wood, W. A.: Recent Observations on Fatigue Failure in Metals. Symposium on Basic Mechanisms of Fatigue, Am. Soc. Test. Mater. Spec. Tech. Publ. (237), 1958, pp. 110-119.

4. Forsyth, P. J. E.: A Two-Stage Process of Fatigue-Crack Growth. Proceedings Crack Propagation Symposium, Cranfield, 1961, pp. 76-94.

5. Coffin, L. F., Jr.: The Concept of Frequency Separation in Life Prediction for Time-Dependent Fatigue. ASME-MPC Symposium on Creep-Fatigue Interaction, MPC-3, R. M. Curran, ed., ASME, 1976, pp. 349-363.

6. Manson, S. S.; and Hirschberg, M. H.: Crack Initiation and Propagation in Notched Fatigue Specimens. 1st International Conference on Fracture, vol. 1, T. Yokobori, T. Kawasaki and J. L. Swediow, eds., Japanese Society for Strength and Fracture of Materials (Sendai, Japan), 1966, pp. 479-498.

7. Paris, P. C.: The Fracture Mechanics Approach to Fatigue. Fatigue, An Interdisciplinary Approach, J. J. Burke, N. L. Reed, and V. Weiss, eds., Syracuse University Press, 1964, pp. 107-127.

8. Ostergren, W. J.: Correlatior of Hold Time Effects in Elevated Temperature Low Cycle Fatigue using a Frequency Modified Damage Function. ASME-MPC Symposium on Creep-Fatigue Interaction, MPC-3, R. M. Curran, ed., ASME, 1976, pp. 179-202.

9. Majumdar, S.; and Maiya, P. S.: A Mechanistic Model for Time-Dependent Fatigue. J. Eng. Mater. Technol., vol. 102, no. 2, Jan. 1980, pp. 159-167.

10. Components in Elevated Temperature Service. CODE CASE N-47-19, Cases of ASME Boiler and Pressure Vessel Code, Nuclear Components, ASME, New York, 1981.

11. Manson, S. S.; Halford, G. R.; and Hirschberg, M. H.: Creep-Fatigue Analysis by Strainrange Partitioning. First Symposium on Design for Elevated Temperature Environment, S.Y. Zamrik, ed., ASME, 1971, pp. 12-24, Disc., pp. 25-28.

12. Manson, S. S.: The Challenge to Unify Treatment of High Temperature Fatigue - A Partisan Proposal Based on Strainrange Partitioning. Fatigue at Elevated Temperatures, A. E. Carden, A. J. McEvily, and C. H. Wells, eds., Am. Soc. Test. Mater. Spec. Tech. Publ. (520), 1973, pp. 744-782.

13. Halford, G. R.; and Nachtigall, A. J.: The Strainrange Partitioning Behavior of an Advanced Gas Turbine Disk Alloy, AF2-1DA. J. Aircraft, vol. 17, no. 8, Aug. 1980, pp. 598-604.

14. Hordon, M. J.: Fatigue Behavior of Aluminum in Vacuum. Acta Metall., vol. 14, no. 10, 1966, pp. 1173-1178.

15. Manson, S. S.; and Zab, R.: A Framework for Estimation of Environmental Effect in High Temperature Fatigue. Environmental Degradation of Engineering Materials, M. R. Louthan, Jr., and R. P. McNitt, eds., Virginia Polytechnic Institute and State University, 1978, pp. 757-770.

16. Sheffler, K. D.; and Doble, G. S.: Influence of Creep Damage on the Low-Cycle Thermal-Mechanical Fatigue Behavior of Two Tantalum Base Alloys. (TRW-ER-7592, TRW Equipment Labs; NASA Contract NAS3-13228.) NASA CR-121001, May 1972.

17. Snowden, K. U.; Stathers, P. A.; and Hughes, D. S.: Grain-Boundary Migration in Metals Fatigued at High Temperatures. Nature, vol. 261, no. 5558, May 1976, pp. 305-306.

18. Annis, C. G.; VanWanderham, M. C.; and Wallace R. M.: Strainrange Partitioning Behavior of an Automotive Turbine Alloy. (FR-7424, Pratt and Whitney Aircraft; NASA Contract NAS3-18930.) NASA CR-134974, Feb. 1976.

19. Halford, G. R.; Saltsman, J. F.; and Hirschberg, M. H.: Ductility Normalized-Strainrange Partitioning Life Relations for Creep-Fatigue Life Prediction. Environmental Degradation of Engineering Materials, M. R. Louthan, Jr. and R. P. McNitt, eds., Virginia Polytechnic Institute and State University, 1978, pp. 599-612.

20. Fine, M. E.; and Ritchie, R. O.: Fatigue Crack Initiation and Near-Threshold Crack Growth. Fatigue and Microstructure, ASM, 1978, pp. 245-278.

21. Thompson, N.; Wadsworth, N. J.; and Louat, N.: Origin of Fatigue Fracture in Copper. Philos. Mag., vol. 1, no. 2, Feb. 1956, pp. 113-126.

22. Taira, S.; Fujino, M.; and Yoshiko, M.: Grain Boundary Sliding in Isothermal and Thermal Fatigue of 304 Stainless Steel. Zairyo (J. Soc. Mater. Sci., Kyoto), vol. 27, no. 296, 1978, pp. 447-453.

23. Michel, D. J.; Nahm, H.; and Moteff, J.: Deformation Induced Twin Boundary Crack Formation in Type 304 Stainless Steel. Mater. Sci. Eng., vol. 11, 1973, pp. 97-102.

24. Mullendore, A. W.; and Grant, N. J.: Grain Boundary Behavior in High Temperature Deformation and Fracture. Proc. of 8th Sagamore Ordinance Materials Research Conference, 1961, pp. 151-205.

25. Oldrieve, R. E.: Fractographic Evalution of Creep Efforts on Strain-Controlled Fatigue-Cracking of AISI 304 LC and 316 Stainless Steel. NASA TM-78913, June 1978.

26. Majumdar, S.; and Maiya, P. S.: A Unified and Mechanistic Approach to Creep-Fatigue Damage. Second International Conference of Mechanical Behavior of Materials, ASM, 1978, pp. 924-928.

27. Priest, R. H.; and Ellison, E. G.: Estimation of Cyclic/Creep Damage by Strain and Strain Rate Considerations. International Conference on Engineering Aspects of Creep, vol. 1, MEP, 1980, pp.185-192.

28. Manson, S. S.; and Halford, G. R.: Practical Implementation of the Double-Linear Damage Rule and Damage Curve Approach for Treating Cumulative Fatigue Damage. Int. J. Fracture, vol. 17, no. 2, 1981, pp. 169-192.

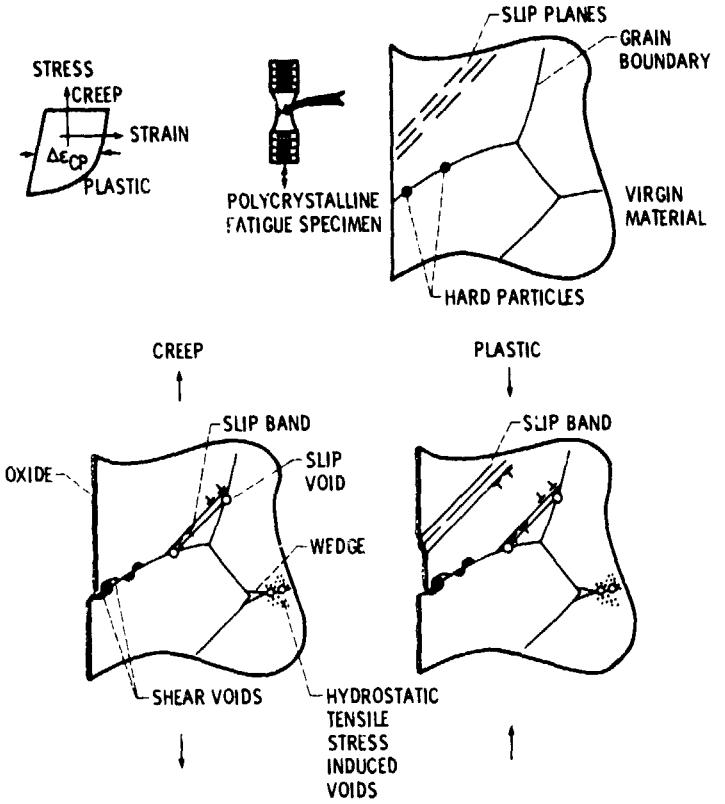

Figure 1. - Cyclic deformation model for Strainrange Partitioning CP cycle.

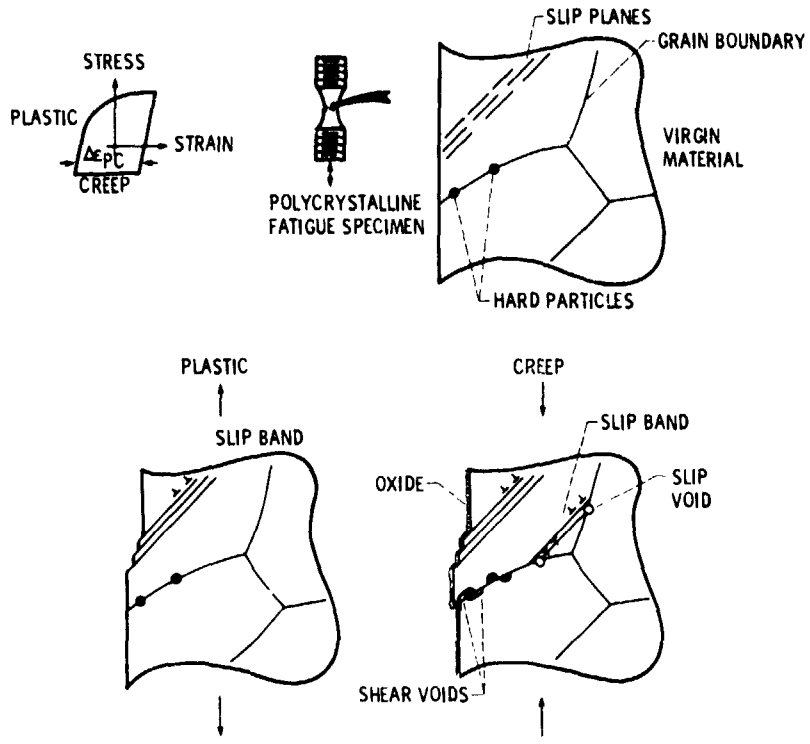

Figure 2. - Cyclic deformation model for Strainrange Partitioning PC cycle.

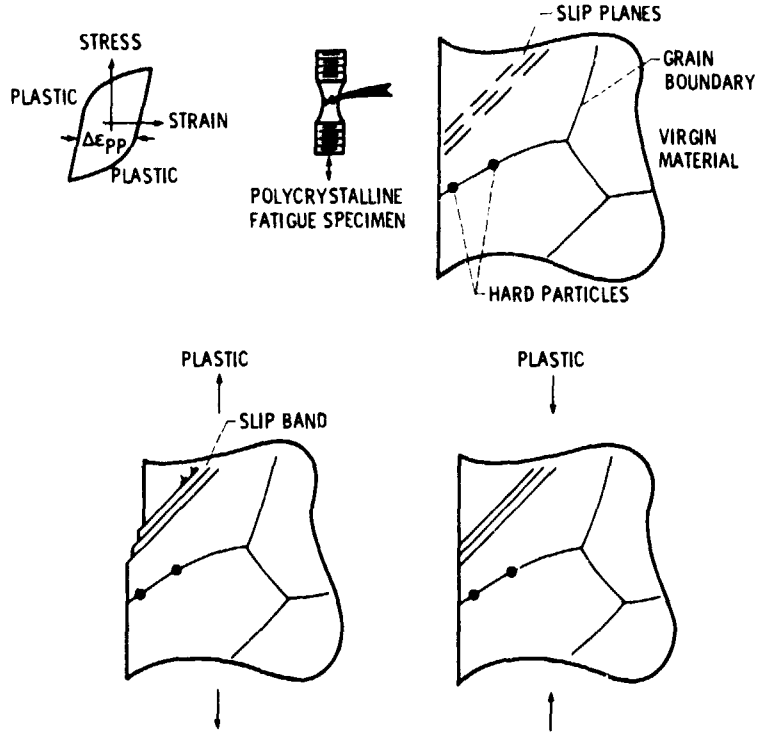

Figure 3. - Cyclic deformation model for Strainrange Partitioning PP cycle.

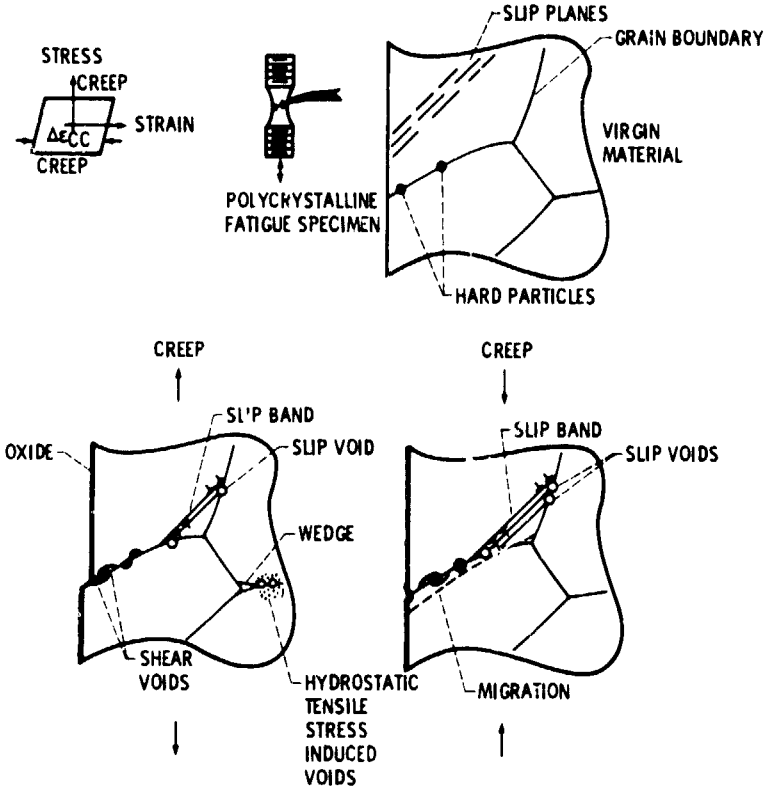

Figure 4. - Cyclic deformation model for Strainrange Partitioning CC cycle.

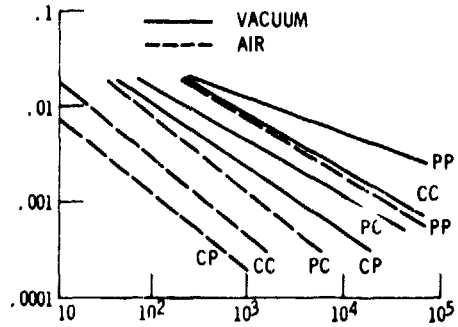

(a) Effect of environment on SRP relations of A-286, 538°-760° C.

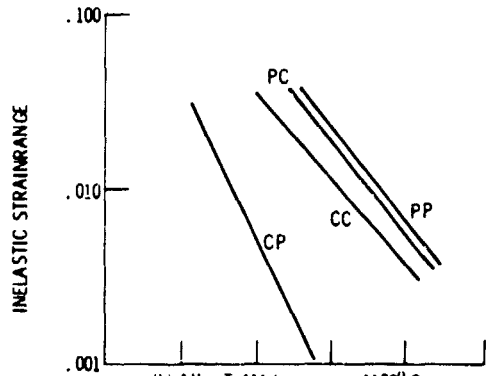

(b) Alloy T-111 (vacuum), 1150° C.

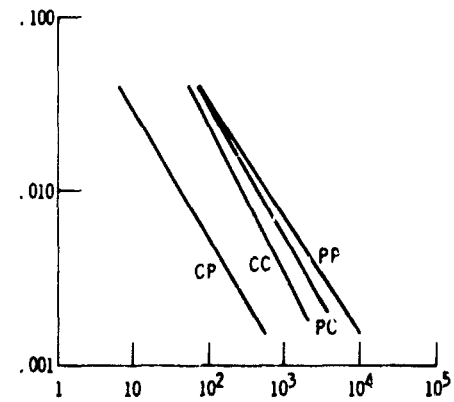

(c) Alloy 316 stainless steel, 705° C.

Figure 5. - SRP life relations for various alloys.

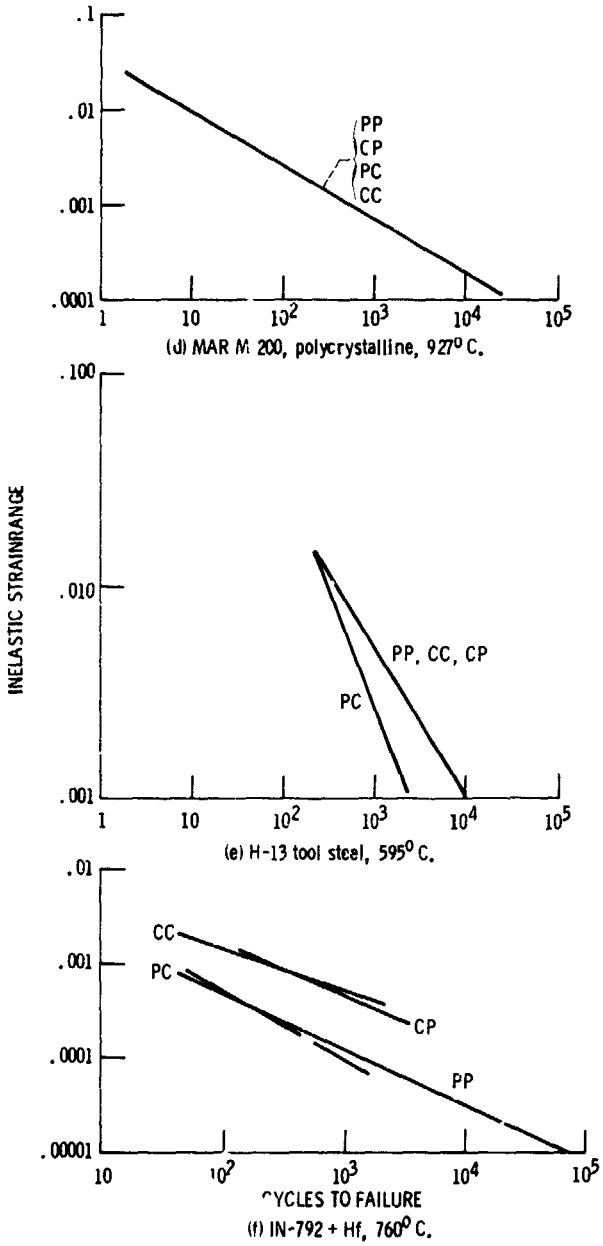

Figure 5. - Concluded.

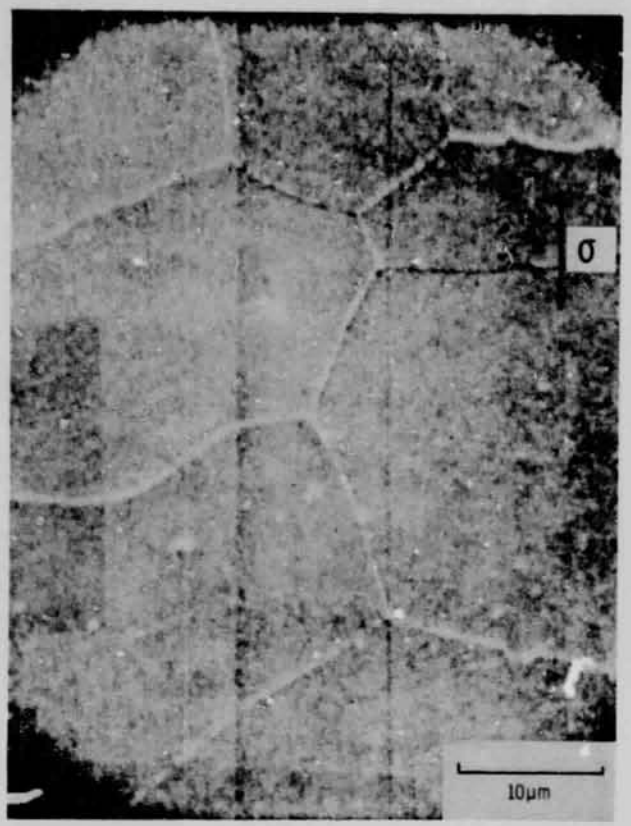

(a) Virgin material.

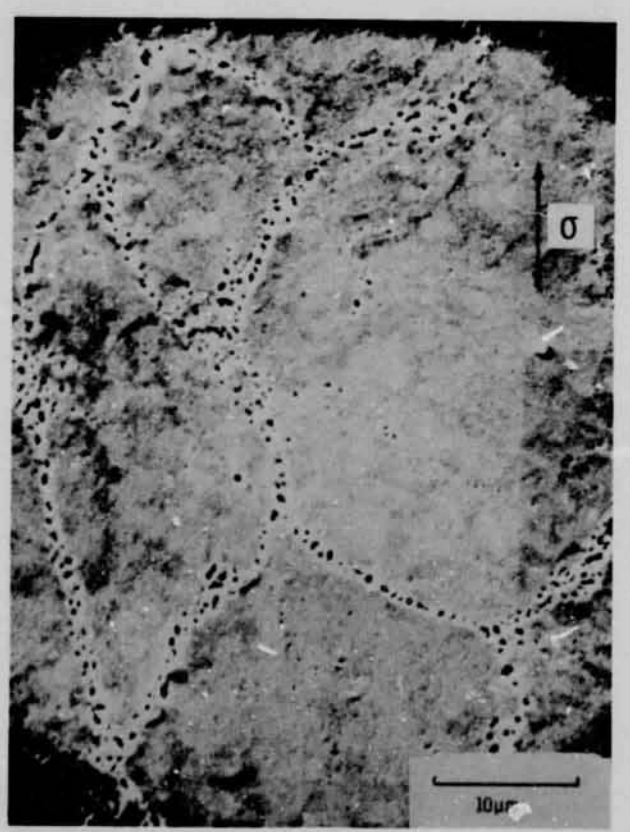

(b) PC loading.

Figure 6. - Creep-fatigue damage in T-111 in high vacuum (10^{-8} torr).

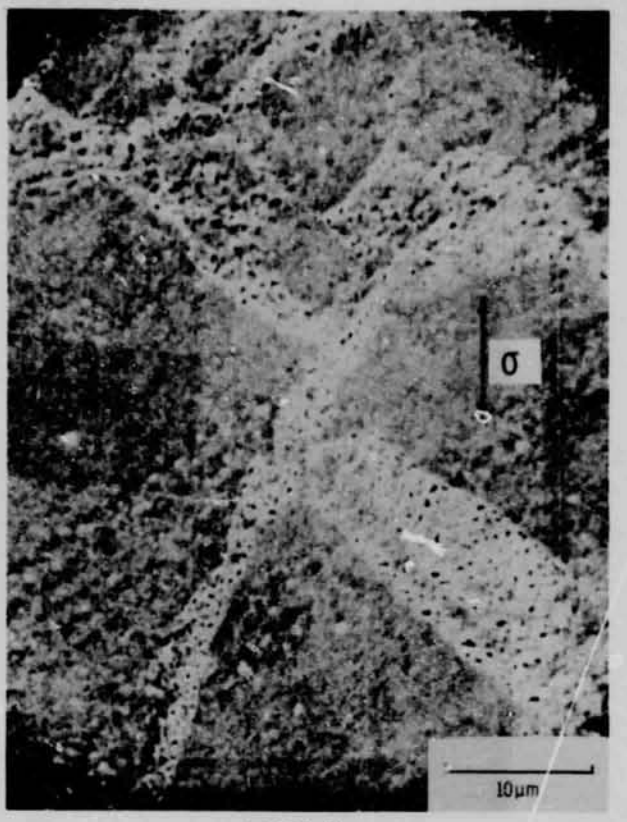

(c) CC loading.

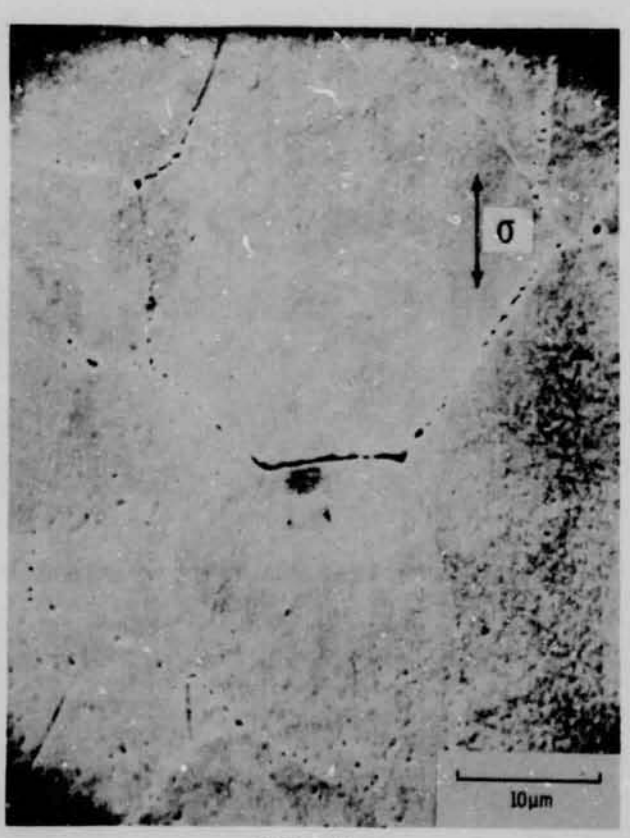

(d) CP loading.

Figure 6. - Concluded.

(a) Room temperature.

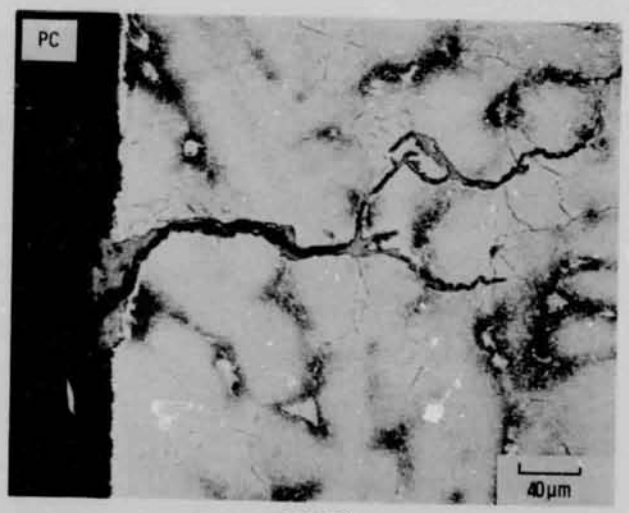

(b) 1700° F.

Figure 7. - Examples of creep-fatigue cracking, cast MAR M 200.

(c) 1700° F.

(d) 1700° F.

Figure 7. - Concluded.

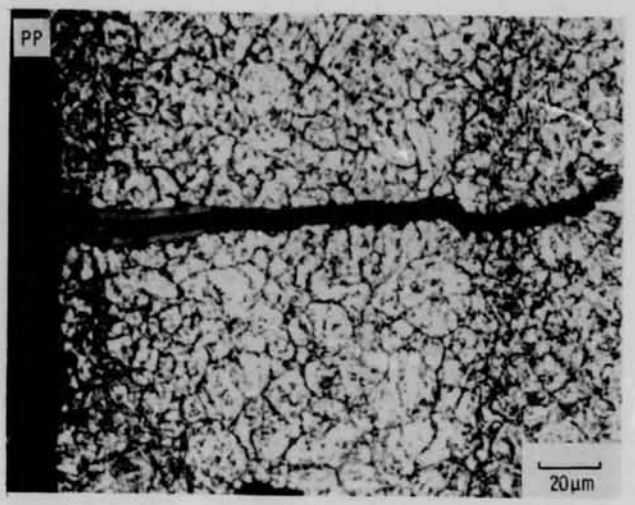

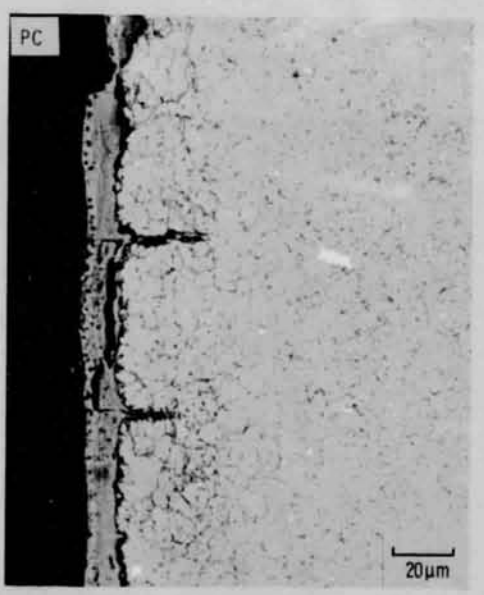

Figure 8. - Examples of creep-fatigue cracking, H-13 tool steel, 1100° F.

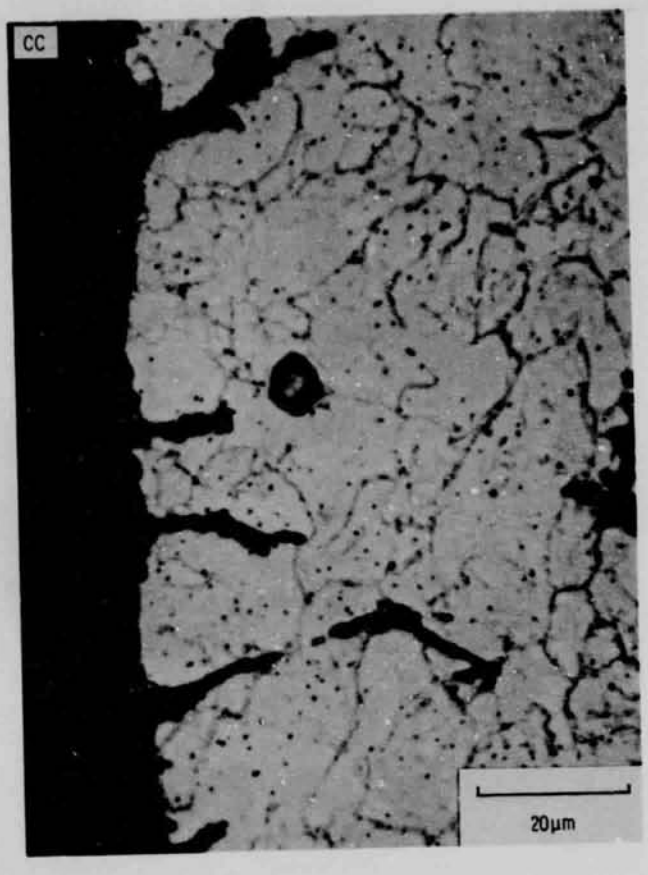

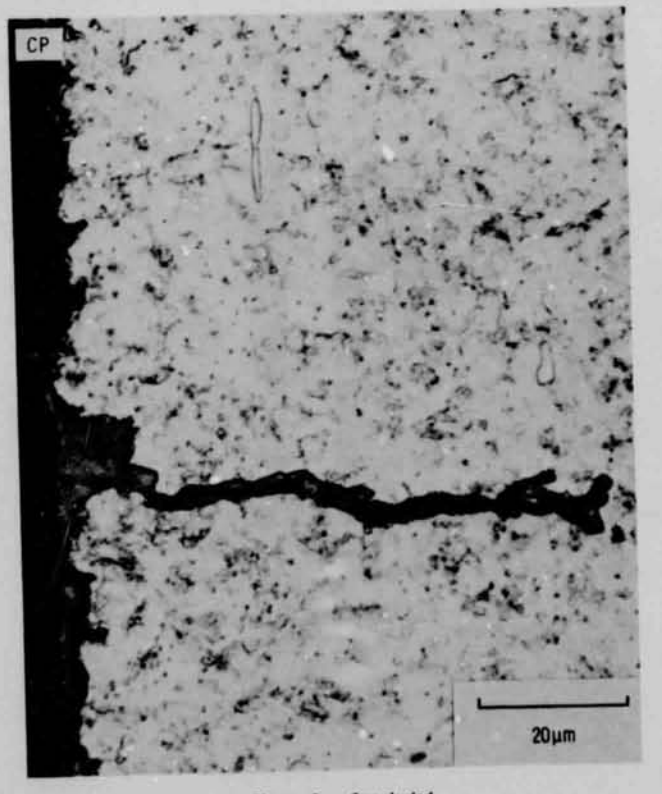

Figure 8. - Concluded.

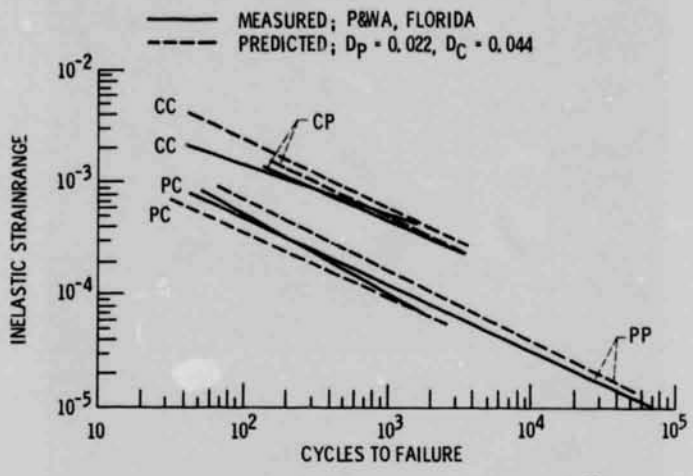

Figure 9. - SRP life relationships for IN-792 + Hf, 760° C.

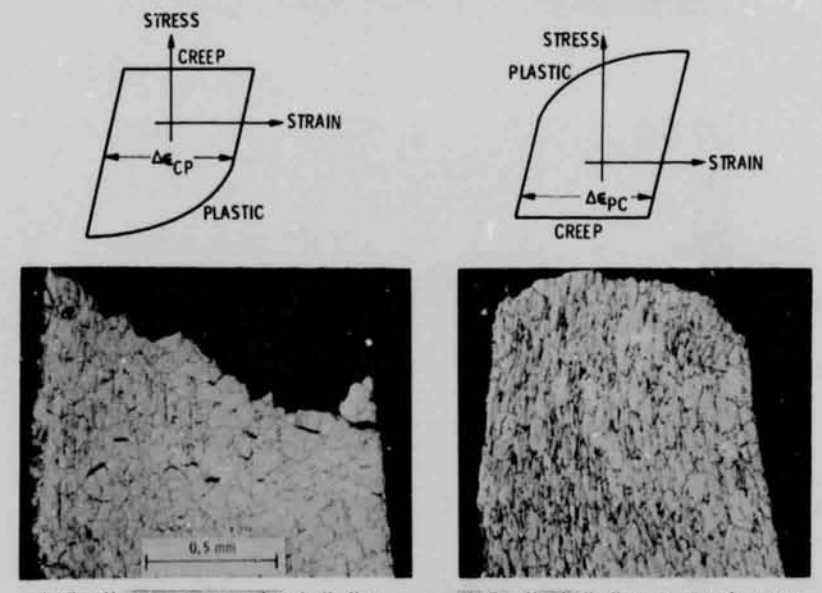

(a) Tensile creep, compressive plastic flow. $\Delta\epsilon_{cp}$ = 0.0147, N = 15. (intergranular).

(b) Tensile plastic flow, compressive creep. $\Delta\epsilon_{cp}$ = 0.0162, N = 264. (transgranular).

Figure 10. - Creep-fatigue fractures in 316SS at 1300° F (approx. 0.5 hr/cycle).

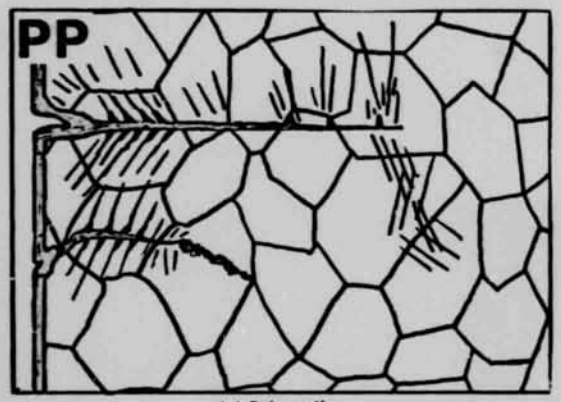

(a) Schematic.

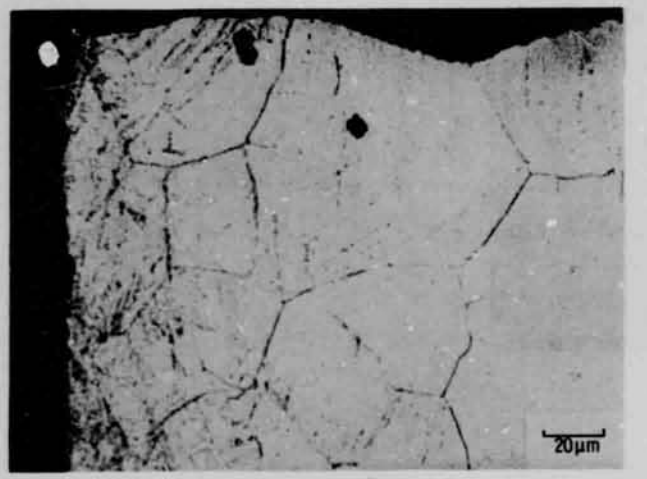

(b) 304 SS, 1200° F

Figure 11. - Examples of PP cracking.

(c) 3166 SS, 1300° F, 20% N_F

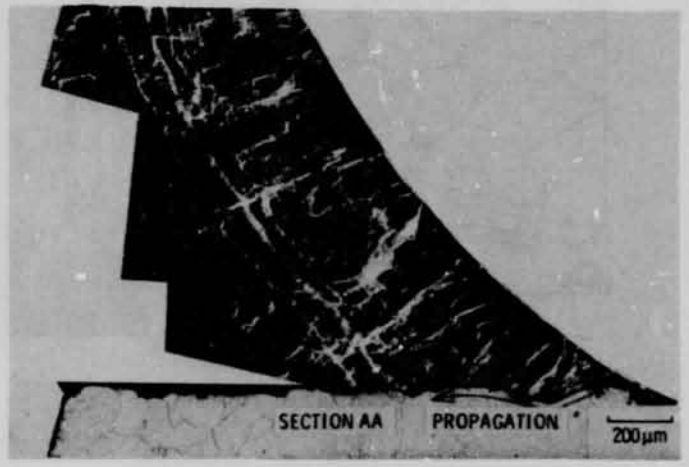

(d) 304 SS, 1200° F

Figure 11. - Concluded.

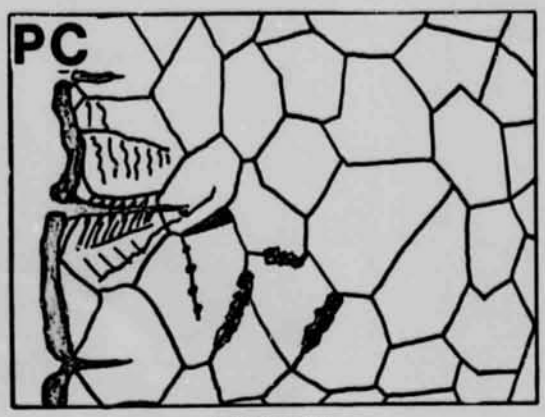

(a) Schematic.

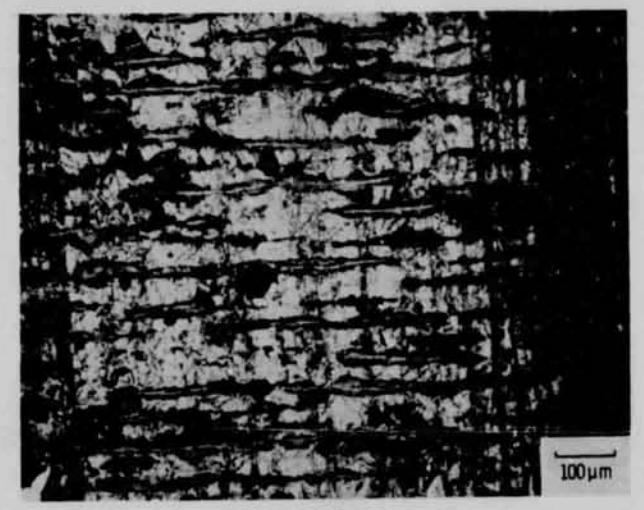

(b) 316SS, 1300° F, 40% N_F.

Figure 12. - Examples of PC cracking.

(c) 316SS, 1300° F.

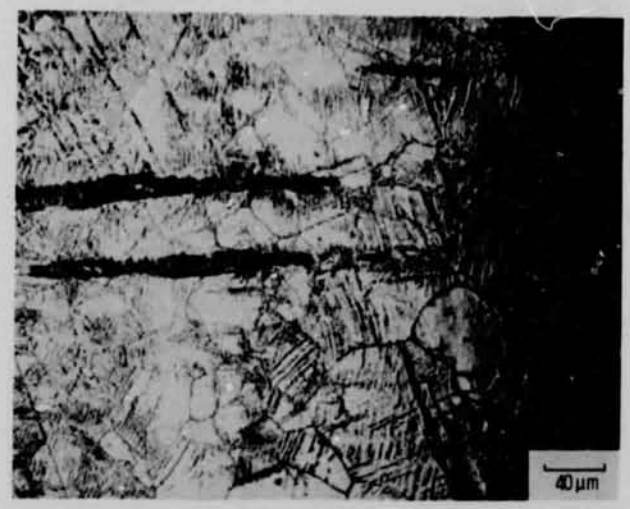

(d) 316SS, 1300° F, 75% N_f.

Figure 12. - Continued.

(e) 316SS, 1300° F.

(f) 304SS, 1200° F, 60% N_F.

Figure 12. - Concluded.

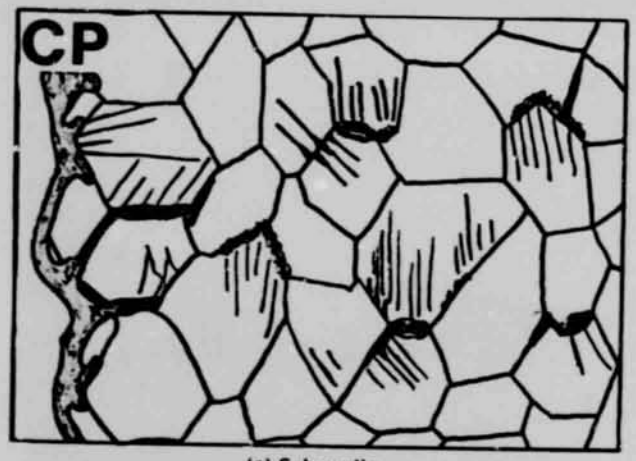

(a) Schematic.

(b) 316SS, 1300° F

Figure 13. - Examples of CP cracking.

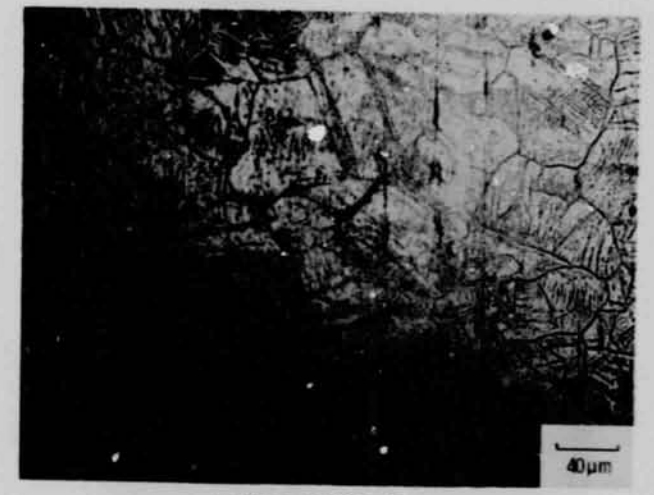

(c) 316SS, 1300° F, 10% N_F

(d) 316SS, 1300° F

Figure 13. - Concluded.

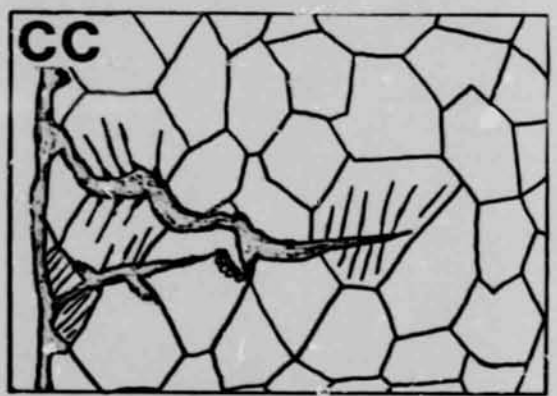

(a) Schematic.

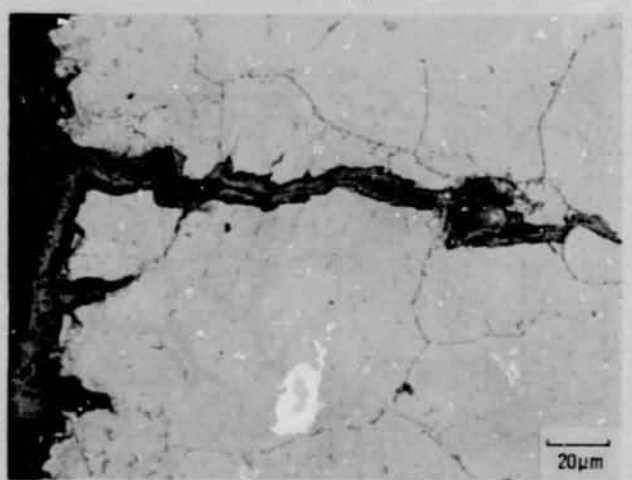

(b) 304SS, 1200^{0} F.

Figure 14. - Examples of CC cracking.

(c) 316SS, 1300^{0}F, 50% N_F.

(d) 316SS, 1300^{0}F, 50% N_F.

Figure 14. - Concluded.

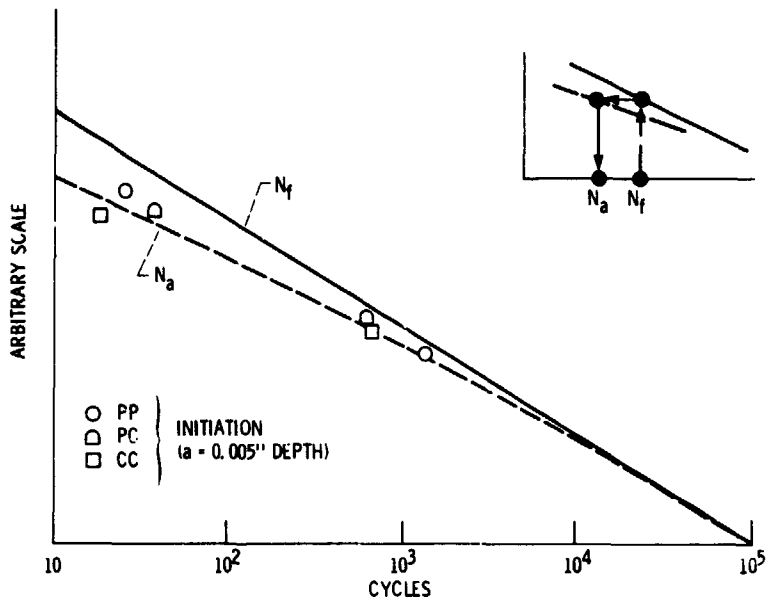

Figure 15. - Crack initiation/failure nomograph applied to SRP, 316 SS, 1300° F.

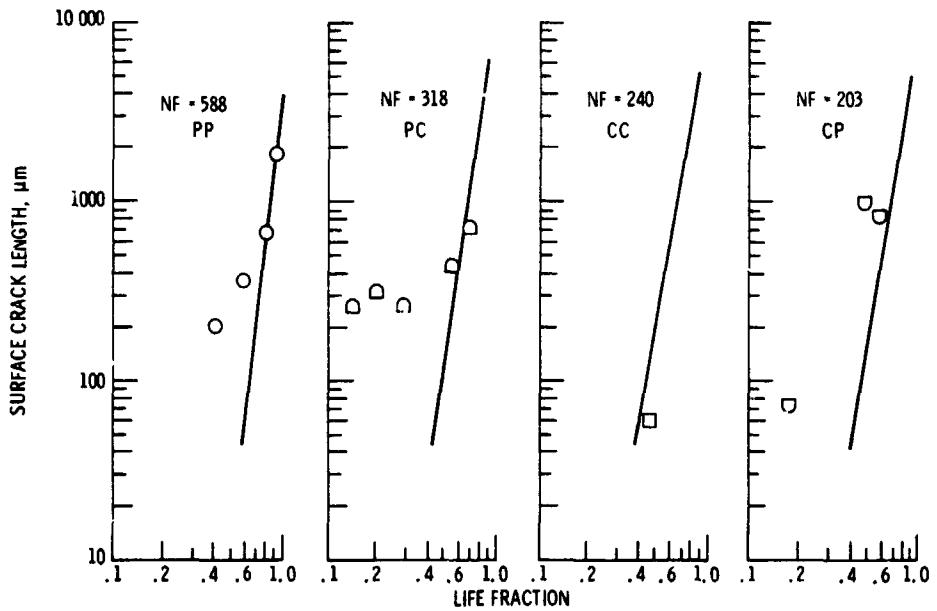

Figure 16. - Surface crack growth for SRP cycles, 316 SS 1300° F.

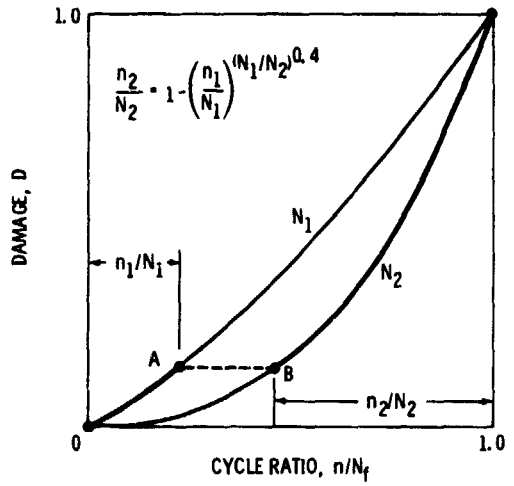

Figure 17. - Damage curve concept for two levels of loading.

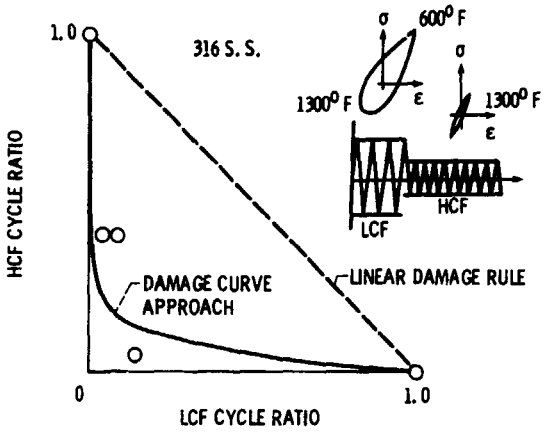

Figure 18. - HCF/LCF interaction at high temperature.